Analysis of FSW Macro-Sections in Aluminum Relative to Unit-Area Analysis

Kevin Colligan
Concurrent Technologies Corporation
Johnstown, PA, USA

Keywords: Joining, Aluminum

Abstract

Macro sections from friction stir welds in 25-mm 7075-T6 aluminum were analyzed to study possible relationships between unit-area quantities (such as average flow stress, lateral pressure, shoulder pressure, heat flux and energy density), basic forces, and the internal structure of the welds. Various features of the sections were examined, including stir zone size and shape, distortion of the grain structure outside of the stir zone and the presence of volumetric defects. This analysis was part of a continuing program to develop unit-area analysis as a means of gaining additional insight into the welding process with possible implications for machine learning and advanced welding controls.

Introduction

The examination of macro-etched cross sections from friction stir welds (FSWs) is a common way of directly visualizing the internal structure produced, both for scientific investigations and for welding procedure qualification. For procedure qualification it is often used for assessing the volumetric soundness of a weld and for assessing the completeness of weld penetration, for example. The study of macro sections has also been used to gain insight into the flow of workpiece material as welds are formed. This technique has been augmented by the addition of tracer materials, such as dissimilar alloys or materials, into the joint at different positions [1-10].

Stir zone (SZ) formation is strongly dependent on the design of the welding tool. The original FSW tool designs generally consisted of a smooth, inwardly tapered shoulder and a cylindrical probe with threads and a spherical tip. These tools generally produced a rounded SZ that was significantly wider than the diameter of the probe. The probe style used in the present study employed a flat shoulder with spiral grooves that pull workpiece material toward the center and a frustum-shaped probe with threads and flats and a flat tip. This style offers several advantages, including improved performance in thick-section welding, the ability to weld without tilting the welding tool and improved penetration of the SZ beyond the tip of the probe. The SZ shape produced by this style of tool more closely matches the profile of the probe, implying more efficient transfer of workpiece material made possible by the interaction of the threads and flats with the workpiece.

Features observed in the examination of macro sections can be categorized as arising from geometric sources or from metalworking issues [11]. Geometric sources include remnant oxide, arising from inadequate probe length, joint misalignment or excessive shoulder diameter [12]. A common geometric issue comes from inadequate plunge depth, evidenced by a raised weld crown surface in relation to the surrounding parent material and accompanying internal voids due to the reduction in material volume under the tool, defects produced by low heat input, and inadequate SZ penetration.

Aside from geometric considerations, there are metallurgical and metalworking considerations that produce features that are exposed in macro section examination. Friction stir welding is a bulk metalworking process, and as such, must produce within the workpiece conditions that are within the material's workability limits. At a given processing temperature and stress state, extreme deformation of the material must take place within these limits, which defines the strain and strain rate that are possible without fracture. State-of-stress workability recognizes the importance of hydrostatic stress components for enhancing the workability of a given process. Intrinsic workability deals with the initial microstructure and alloy chemistry of the workpiece, and the changes in microstructure that are produced as part of the metalworking process [13]. Although many metalworking processes and materials have

been extensively studied in relation to the limits of workability, friction stir welding has not yet been adequately subjected to such scrutiny.

Unit-area analysis is being developed as a means of normalizing the basic features of the FSW process with respect to workpiece thickness [14-16]. The goal is to resolve the tool geometry, forces and spindle torque in a way that permits comparison between procedures executed in different material thickness. To facilitate study of different welding procedures, unit-area analysis seeks to convert "global" quantities to "unit-area" quantities. For example, unit-area analysis provides a means to reduce the measured spindle torque to an equivalent uniformly distributed shear stress, then to the equivalent flow stress at the tool/workpiece interface. This may provide an equal basis on which to analyze a diverse collection of welding procedures.

Unit-area analysis depends on mathematically reducing the welding tool geometry to a single quantity, referred to as G (for geometry) [17]. This parameter is calculated as the integral of the radius over the tool/workpiece interface area. The expression for G is dependent on the style of welding tool used. For example, for a flat or tapered shoulder with a flat-tipped, frustum-shaped probe, the expression for G is,

$$G = \frac{2\pi}{3}\left[\frac{S^3 - {P_r}^3}{\cos\alpha} + \frac{t((P_R + P_T)^2 - P_R P_T)}{\cos\beta} + {P_T}^3\right] \tag{1}$$

where,

$\alpha = shoulder\ concavity\ angle$
$\beta = frustum\ probe\ half\ angle$
$S = shoulder\ radius$
$P_R = probe\ root\ radius$
$P_T = probe\ tip\ radius$
$r = dimension\ in\ radial\ direction$
$z = dimension\ along\ probe\ axis$
$t = workpiece\ thickness, or\ probe\ length$
$\theta = anglular\ position$

From this, expressions for the average flow stress, area-based average surface velocity, heat flux and energy density can be derived [16].

To compare welding procedures in terms of spindle speed and welding speed, comparable expressions are used in this work that seek to normalize these basic machine settings in terms of an area-based surface velocity and volume-based travel speed. The average surface velocity is expressed as,

$$\omega\overline{r} = \omega\frac{G}{total\ area} \tag{2}$$

where ω is the angular velocity and $\bar{r}$ is the average radius. The equivalent to welding speed used here is volumetric flowrate, FR, which is simply calculated as

$$FR = vt(P_R + P_T) \tag{3}$$

The unit-area expression used in the present work as an equivalent to spindle torque is flow stress, σ_{flow},

$$\sigma_{flow} = \frac{T\sqrt{3}}{G} \tag{4}$$

where T is the spindle torque. Shoulder pressure, *SP*, is simply the plunge force, F_{plunge}, divided by the shoulder area,

$$\mathrm{SP} = \frac{F_{plunge}}{\pi S^2} \tag{5}$$

where S equals the shoulder radius. The lateral pressure on the probe, *LP*, is expressed as the lateral force divided by the lateral area of the probe. For a frustum-shaped probe with a flat tip, the lateral pressure is,

$$\mathrm{LP} = \frac{\sqrt{\left({F_{longitudinal}}^2 + {F_{transverse}}^2\right)}}{t * (P_r + P_t)} \tag{6}$$

where $F_{longitudinal}$ and $F_{transverse}$ are the longitudinal and transverse forces on the welding tool, respectively. The heat flux is the power output per unit area of the tool/workpiece interface, and is proportional to the average temperature gradient at the interface. The heat flux, ϕ_q, with units of power per unit area, is calculated as,

$$\phi_q = \frac{T}{G} \times \omega \bar{r} \tag{7}$$

Early research in FSW attempted to normalize heat input based on the total power output and the travel speed, yielding "specific energy". However, this formulation did not account for differences possible with respect to workpiece thickness. To improve the expression of the energy put into the workpiece, in terms of volume of processed material, the energy density can be calculated as shown below, with weld pitch calculated as the travel speed divided by the spindle speed. Energy density is proportional to the temperature distribution in the workpiece. Two expressions for energy density are possible. The first expression, ρ_{E1}, is based on the lateral probe area.

$$\rho_{E1} = \frac{\phi_q \times (total\ tool\ area)}{FR} = \frac{2\pi T}{weld\ pitch \times (lateral\ probe\ area)} \text{ (units: energy per unit volume)} \tag{8}$$

There is a second possible expression of energy density, ρ_{E2}, based on the total tool area, is shown below, although it remains to be seen if one expression is superior to the other in terms of data set analysis. This second expression is the version of energy density used in the present work.

$$\rho_{E2} = \frac{\phi_q}{travel\ speed} = \frac{2\pi T}{weld\ pitch \times (total\ tool\ area)} \text{ (units: energy per unit volume)} \tag{9}$$

An additional data feature developed as part of this work is referred to as excess shoulder pressure. This feature seeks to normalize the plunge force based on the flow stress. The excess shoulder pressure, *ESP*, is expressed as the shoulder pressure, *SP*, minus the flow stress, *FS*,

$$ESP = SP - FS \tag{10}$$

The present work is part of a larger effort to develop advanced controls and machine learning techniques to reduce the level of expertise required to implement FSW in a production environment by improvements in machine control. As part of this work, welding experiments that included a wide scope of machine settings were conducted and analyzed with the goal of developing new data features that expressed welding conditions in a way that could be used to advance the program goals. This paper summarizes the analysis of macro sections from these welds and seeks to correlate weld formation with the various data features from unit-area analysis.

Experimental Approach

In this study, welds were made with the objective of mapping the effects of machine settings to a broad variety of results. Unit-area quantities were calculated from the measured axis forces and spindle torque. Post-weld evaluations included visual inspection of the weld crown, quantitative assessment of excess flash production, examination of macro sections, assessments of tensile tests, and inspection from phased-array ultrasonic and

radiographic methods. The macro sections were photographed using a light macroscope at low magnification. The goal was to correlate unit-area quantities with weld outcomes as input to the development of advanced controls and machine learning approaches.

Bead-on-plate welds were made in 25-mm thick by 305-mm wide by 1,016-mm long 7075-T6 aluminum plates that were each bolted to a steel welding fixture. Each weld was made with either constant welding speed or constant spindle speed, according to the experimental plan. The welding tool dimensions are given in Table 1. The two-piece welding tool was adjusted to give a 0.5-mm gap between the pin tip and the anvil.

Four series of welds are presented, as summarized in Table 2. Each series had welds made in position control and in load control, although not all results are presented here. For welds made in position control, where a constant plunge depth was maintained with different machine settings, the measured plunge force was considered an output from the machine spindle speed/travel speed combination. In welds made in load control, the results were regarded as the result from the machine settings at the given plunge force. Each weld was made with between four and six segments of stable machine settings. Subsequent log file data analysis isolated segments of stable input conditions and output forces and average values were calculated from the basic force data which were then used to calculate unit-area analysis quantities of flow stress, heat flux and energy density.

Results

Figure 1 shows a map of the four series of welds made as a function of the basic machine settings of spindle speed and welding speed. Welding conditions that exhibited volumetric defects are circled and trends in macro-section observations are noted in the figure. As expected, extremes of travel speed and spindle speed generally exhibited volumetric defects and variation in tensile strength, as will be discussed below in detailed reviews of the four series of welds. The reviews of each weld series attempt to correlate the macro sections with changes in the unit area quantities.

The average flow stress, energy density and lateral probe pressure for Series 1 welds is shown in Figure 2. These quantities are plotted as a function of average surface velocity, with all welds having been made at a constant welding speed of 1.27 mm/s (535 mm^3/s volumetric flowrate). In this chart the flow stress is seen to trend downward with increasing surface velocity. It has previously been shown [14] that flow stress trends linearly with respect to the inverse of the surface velocity for welds that exhibit a linear trend in heat flux with respect to surface velocity. Interestingly, the lateral pressure on the probe decreased with increasing surface velocity until a surface velocity of about 0.15 m/s, then increased with increasing surface velocity. The energy density and heat flux both increased linearly with respect to surface velocity, except for the procedure that had the lowest surface velocity where the energy density and heat flux were seen to deviate below the linear trend.

A macro section from an exemplary welding procedure is shown in Figure 3. The conditions for this procedure were at the intersection between Series 1 and Series 2 welds, which coincidentally, is approximately at the minimum lateral probe pressure for Series 1. The general structure of the weld section is representative of welds made with this welding tool style, with the stir zone (SZ) boundary approximately following the probe profile, except in the upper portion of the SZ which smoothly blends outward to the shoulder width. It is notable that this style of welding tool produces a SZ that contrasts distinctly from the SZ produced by a welding tool with a cylindrical, threaded probe with no other reentrant features, such as flutes or flats, likely due to very different material flow produced by the different tool styles.

At the very lowest surface velocity in Series 1 a small volumetric defect was found in the lowest portion of the SZ, as shown in Figure 4. Under higher magnification it appeared that a remnant of thread-shaped material could be seen inside the cavity, suggesting that the source of this defect was interruption of the normal consumption of the keyhole wall by extreme plastic deformation behind the advancing tool. The fact that this procedure exhibited energy density that was below the linear trend from higher surface velocities and high flow stress further supports the idea of inadequate plastic deformation, possibly due to low local temperature at the bottom of the weld.

In Series 1, at surface velocities above about 0.16 m/s, all macro sections exhibited upturned grains in the thermomechanically affected zone (TMAZ) just outside of the SZ. Welds made at 0.178 m/s surface velocity (167 rev/min spindle speed) and higher also exhibited non-uniform structure in the upper SZ, as shown in Figure 5. Welds at 227 rev/min spindle speed (0.241 m/s surface velocity) and higher all exhibited large voids in the upper stir zone which were packed with discontinuous fragments of parent material, as shown in Figure 6. Post-weld visual inspection of the welds indicated a "surface tearing" appearance, but macro sections revealed that these voids were more extensive than a surface defect. It was also noted that these voids extended deeper into the weld as the surface velocity increased.

Welds above 0.16 m/s surface velocity also exhibited a distinct change in SZ shape in the shoulder region. Figure 7 shows the sudden change in the shape of the upper advancing side of the SZ. At 0.157 m/s surface velocity and less, the SZ shape more smoothly transitions from the shoulder outside diameter to the pin profile shape. At 0.178 m/s surface velocity and above there was a sudden narrowing of the upper portion of the advancing side SZ, ultimately resulting in the shoulder producing very little SZ material, as seen for example in Figure 6.

The average flow stress, energy density, lateral probe pressure, heat flux and excess shoulder pressure for Series 2 welds, made at a surface velocity of 0.157 m/s (148 rev/min spindle speed), are shown in Figure 8. The welds reported here were made in position control. The only volumetric defect observed in the welds from Series 2, shown in Figure 9, was from a procedure at the lowest welding speed. In that weld, a broad region of the upper SZ contained numerous, small volumetric defects. There was also a much shallower penetration of stir zone material from the shoulder, visible in the figure and similar to that shown in Figure 7 (right side). The macro sections from welds made at below 450 mm^3/s volumetric flowrate all exhibited upturned grains in the TMAZ just outside of the SZ, similar to that shown in Figure 5.

Series 2 welds exhibited the highest tensile strength values of all the welds produced. The highest tensile strength, 439 MPa, was produced at a volumetric flowrate of about 800 mm^3/s (1.91 mm/s welding speed) and 0.157 m/s surface velocity (148 rev/min spindle speed). In that weld segment, the flow stress was 43.3 MPa. A macro section from that segment is shown in Figure 10.

The average flow stress, energy density, lateral probe pressure, heat flux and excess shoulder pressure for Series 3 welds, made at a surface velocity of 0.095 m/s (89 rev/min spindle speed), are shown in Figure 11. Welds were made in load control only in this series of welds. Defects were observed on the advancing side of the SZ in all welds made at about 600 mm^3/s volumetric flowrate (1.48 mm/s welding speed) and higher, and additional defects in the root of the SZ were observed in welds made at a volumetric flowrate of about 800 mm^3/s (1.91 mm/s welding speed) and higher. Examples of each type of defect are shown in Figure 12 and Figure 13, respectively.

The average flow stress, energy density, heat flux, lateral probe pressure and excess shoulder pressure for Series 4 welds, made at a surface velocity of 0.241 m/s (227 rev/min spindle speed), are shown in Figure 14. Welds were made in load control only in this series of welds. All welds made in this series exhibited defects in the upper SZ, similar to that shown in Figure 6, which were visible at the time of welding. It is notable that as the travel speed increased, the severity of the defects decreased.

Discussion

From these results it appears that average flow stress, calculated from tool geometry and spindle torque, is a reasonable indicator of defect formation for the tools and materials tested. In Series 1, as the surface velocity increased and the flow stress dropped to about 32 MPa, initial irregularities in the upper SZ were observed. As the flow stress dropped further in that series with increasing surface velocity, these indications worsened, eventually leading to volumetric defects at a flow stress of about 26 MPa. These defects increased in depth as the surface velocity increased and the flow stress decreased further. It does not appear that surface velocity is a sufficient indicator of weld quality for upper SZ defects in this range of machine settings. In Series 4 the upper SZ defects observed at low travel speed reduced in severity as the welding speed increased while the flow stress was also increasing, up to about 29 MPa, at constant surface velocity. Figure 15 shows a contour plot of flow stress as a

function of machine settings, overlaid with indications of procedures that had volumetric defects. Welding procedures with average flow stress above roughly 55 MPa and below roughly 30 MPa exhibited defects.

The results from welding Series 2, shown in Figure 2, showed that as the spindle speed increased from a low value the lateral probe pressure decreased until a minimum value was reached at about 0.15 m/s surface velocity. As the surface velocity was increased further the lateral pressure increased continuously. A similar result was predicted by simulation results [18]. It is speculated that this effect can be explained as follows. At low rotational speed, the rotation of the tool is too slow to assist in transporting material around the probe for the given travel speed. At such low spindle speeds material transport is dominated by extrusion, which explains the high lateral force. As the spindle speed increases, rotation of the probe contributes more to material transport, thus the decreasing lateral force, until a minimum force value is reached. The surface velocity that produces minimum lateral force can be considered an optimum value in terms of the efficiency of material transport which minimizes the dependence on extrusion for material transport. In the present study this was observed between 0.136 m/s and 0.157 m/s average surface velocity. With increasing surface velocity, the flow stress was seen to continue to decrease, suggesting increased thermal softening of the workpiece. As the surface velocity was increased above the optimum value, it is speculated that further increase in thermal softening reduced the rotational drag of material around the probe, resulting in a return to material flow dominated by extrusion and with that, increased lateral force. Evidence of this extrusion on the retreating side of the SZ is seen in Figure 5 and Figure 6.

It is possible that the degradation of weld quality at surface velocities above the optimum value arise from a combination of state-of-stress workability and intrinsic workability failures. Increasing the surface velocity reduces the flow stress and presumably increases the peak temperature at the tool/workpiece interface. Increased surface velocity also is expected to increase the strain rate at the interface, simply because the features of the welding tool that induce plastic deformation are moving at increasing velocity. The state of stress may also play a role. In welds made with no shoulder (unpublished work), forward motion of the pin produced upwelling and loss of material in front of the pin. With the shoulder present, this tendency of the probe to push material upward may result in compression of material upward against the shoulder, which should produce some amount of hydrostatic stress against the shoulder and against the leading edge of the probe, reducing the tendency to fracture the material as it is deformed. As the surface velocity increases, with constant welding speed, this hydrostatic stress may become reduced, resulting in material fracture. Other mechanisms are possible, such as fracture initiating in the region behind the probe, where upwelling is not expected to play a role. Further experimental investigation is needed to properly explain this type of defect formation.

Defect formation at low surface velocity appeared to be of a different nature. At a surface velocity of 0.095 m/s and volumetric flowrates above 535 mm^3/s voids initially appeared at the advancing side SZ/TMAZ boundary, which increased in severity with increasing welding speed. In this region of machine settings, summarized in Figure 2, flow stress values were observed to be the highest of all welds made, in the range of 50 to 60 MPa (Figure 11 and Figure 15), and the energy density was observed to be very low, in the range of 2.1 to 1.6 W/mm^2. The implication here is that the peak temperature is very low, resulting in high flow stress, and the temperature distribution is low (low energy density). Considering that the voids were located on the extreme advancing side of the SZ, combined with the low peak temperature and possibly low temperature just outside of the SZ, suggest the possibility of cooling-interrupted coalescence of material as it is flowing forward to fill the advancing side void behind the probe. The irregular, jagged shape of the voids suggest thread-formed material cooling before full consolidation is achieved. As the welding speed is further increased, the appearance of voids in the root of the SZ suggest that cooling from the anvil and possibly low local surface velocity at the tool/workpiece interface, caused voids to appear there.

Conclusions

In this work, friction stir welds were systematically made in thick-section 7075-T6 to explore the correlation between the basic machine settings of spindle speed and travel speed, weld quality and to explore correlation of welding quality with unit-area analysis techniques. It was generally found that the average flow stress at the tool/workpiece interface, calculated from the spindle torque and welding tool geometry, was a reasonable predictor

of weld quality in terms of volumetric defects. Welds in the range of 55 to 30 MPa were found to be volumetrically sound. Welds with lower average flow stress exhibited volumetric defects in the upper SZ, which increased in severity with decreasing flow stress. Welds with average flow stress above 55 MPa exhibited defects in the advancing side SZ/TMAZ boundary and SZ root, which it is speculated is due to cooling-interrupted coalescence of material as it is pushed forward to fill the gap behind the pin on the advancing side. More experimental work, possibly using stop-action methods, may explain these defects in greater detail.

References

1. Colligan, K.J., "Dynamic Material Deformation During Friction Stir Welding in Aluminum*," Proc. 1st Int. Sym. on Friction Stir Welding*, The Welding Institute, Thousand Oaks, USA 1999.
2. Colligan, K.J., "Material Flow Behavior During Friction Stir Welding," *Welding Journal*, July 1999.
3. Guerra, M., McClure, J.C., Murr, L.E., and Nunes, A.C., "Metal Flow During Friction Stir Welding," *Friction Stir Welding and Processing*, TMS, 2001.
4. McClure, J.C., Coronado, E., Aloor, S., Nowak, B.M., Murr, L.E., and Nunes, Jr., A.C., "Effect of Pin Tool Shape on Metal Flow During Friction Stir Welding," *Proc. 6th Int. Conf. on Trends in Welding Research*, April 15-19, 2002, Pine Mountain, GA, USA.
5. Dickerson, T., Shercliff, H.R., and Schmidt, H., "A Weld Marker Technique for Flow Visualization in Friction Stir Welding," *Proc. 4rth Int. Sym. on Friction Stir Welding*, The Welding Institute, Park City, Utah, 2003.
6. Reynolds A.P., Seidel, T.U., and Simonsen, M., "Visualization of Material Flow in an Autogenous Friction Stir Weld," *Proc. 1st Int. Sym. on Friction Stir Welding*, The Welding Institute, Thousand Oaks, USA 1999.
7. Seidel, T.U. and Reynolds, A.P., "Visualization of the Material Flow in AA2195 Friction Stir Welds Using a Marker Insert Technique," *Metallurgical and Materials Transactions A*, 32A, 2001.
8. London, B., Mahoney, M., Bingle, W., Calabrese, M., and Waldron, D., "Experimental Methods for Determining Material Flow in Friction Stir Welds," *," Proc. 3rd Int. Sym. on Friction Stir Welding,* The Welding Institute, Kobe, Japan, 2001.
9. Ouyang, J.H., Kovacevic, R., Jandric, D., Song, M., and Valant, M., "Visualization of Material Flow During Friction Stir Welding of the Same and Dissimilar Aluminum Alloys," *Proc. 6th Int. Conf. on Trends in Welding Research*, April 15-19, 2002, Pine Mountain, GA, USA.
10. London, B., Mahoney, M., Bingel, W., Calabrese, M., Bossi, R.H., and Waldron, D., "Material Flow in Friction Stir Welding Monitored with Al-SiC and Al-W Composite Markers," *Friction Stir Welding and Processing II*, TMS, 2003.
11. Arbeghast, W.J., "A Flow-Partitioned Deformation Zone Model for Defect Formation During Friction Stir Welding," Scripta Materialia, V. 58, Issue 5, pp. 372-376, 2008.
12. Colligan, K.J., "Description of a Pre-Rotation Defect in Friction Stir Welding of 5456 Aluminum, *Proc. 8th Int. Sym. On Friction Stir Welding*, The Welding Institute, Timmendorfer Strand, Germany 18-20 May, 2010.
13. Hot Working Guide, eds. Prassad, Y.V.R.K., Rao, K.P. and Sasidhara, S., 2nd edition, ASM International, 2015.
14. Colligan, K., "Analysis of data from friction stir welds in aluminum," *2022 International Symposium on Friction Stir Welding and Processing*, Luneburg, Germany, 28-30 September, 2022.
15. Colligan, K., "Analysis of Torque Data from Friction Stir Welds in Aluminum Alloys," Friction Stir Welding and Processing XII, TMS Annual Meeting, San Diego, California, March 19-23, 2023.
16. Colligan, K., "Unit-Area Analysis of Friction Stir Welding Data," Proc. 13th Int. Sym. On Friction Stir Welding and Processing, The Welding Institute, Kyoto, Japan, May 21-23, 2024.
17. Andrade, D.G., Leitao, C., Dialami, N., Chiumenti, M. and Rodrigues, D.M., "Modelling Torque and Temperature in Friction Stir Welding of Aluminum," *Int. Journal of Mechanical Sciences*, Vol. 182, 16 May, 2020.
18. Long, T. and Reynolds, A.P., "Parametric Studies of Friction Stir Welding by Commercial Fluid Dynamics Simulation," *Science and Technology of Welding and Joining*, Vol. 11, No. 2, pp. 200-208, 2006.

Table 1. Welding tool details.

Shoulder material	Viscount 44 (resulferized H13 tool steel)
Pin material	MP-159 (Co-Ni)
Shoulder description	Flat, three spiral scrolls
Pin description	Frustum, flat tip, threaded (1.81 mm pitch) with 5 flats
Shoulder diameter	35.56 mm
Pin root diameter	21.01 mm (typical)
Pin tip diameter	12.7 mm
Pin length	24.94 mm (typical)
G	2.14EE-5 m^3
Total tool surface area	2.11EE-3 m^2

Table 2. Basic machine settings for four welding test series.

Test Series	Spindle Speed – Surface Velocity Range	Welding Speed – Volumetric Flowrate Range
	rev/min (m/s)	mm/s (mm^3/s)
1	70 - 305 (0.075 – 0.32)	1.27 (535)
2	148 (0.157)	0.42 – 2.12 (178 – 893)
3	89 (0.095)	0.64 – 2.12 (266 – 893)
4	227 (0.241)	0.64 – 1.91 (266 – 801)

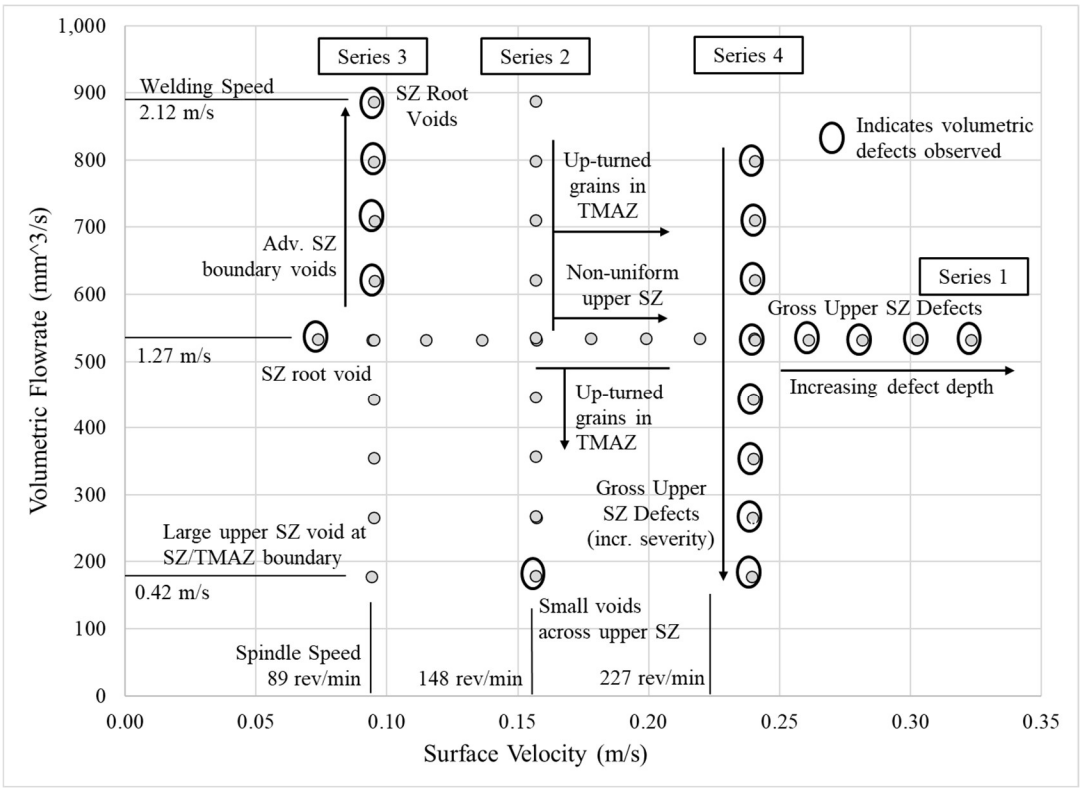

Figure 1. Summary of welds made in 25-mm 7075-T6 aluminum with notations of volumetric defects observed.

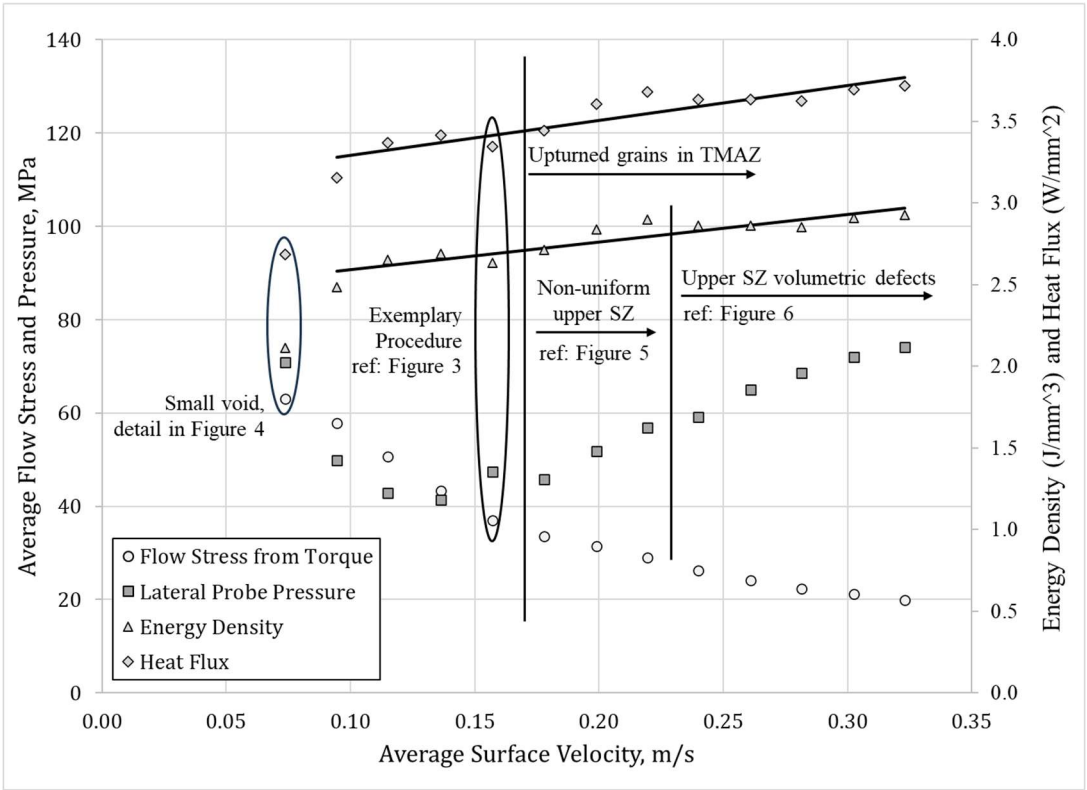

Figure 2. Test Series 1 average flow stress, lateral probe pressure and energy density as a function of average surface velocity, from welds in 25-mm 7075-T6 aluminum, all made at 1.27 mm/s travel speed (535 mm^3/s volumetric flowrate).

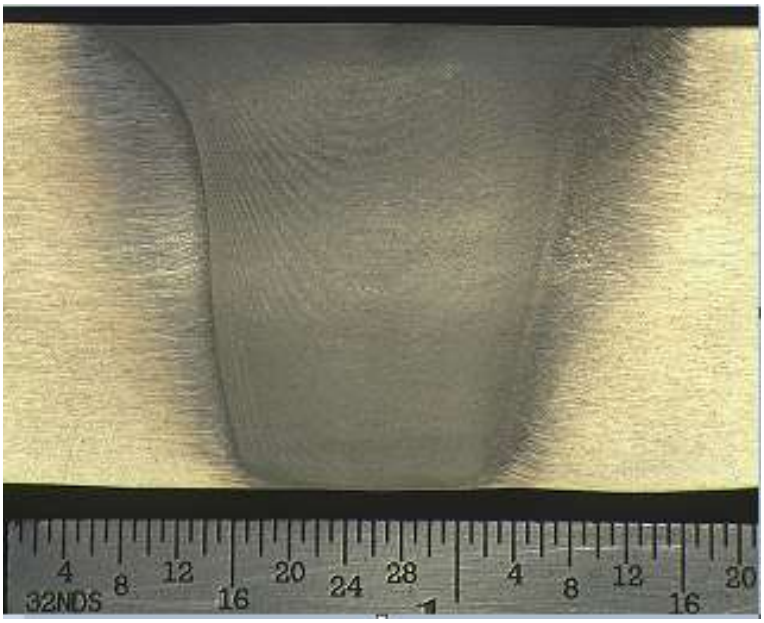

Figure 3. Macro section from an exemplary weld in 7075-T6 aluminum, made at 148 rev/min spindle speed (0.157 m/s average surface velocity) and 1.27 mm/s travel speed (535 mm^3/s volumetric flowrate).

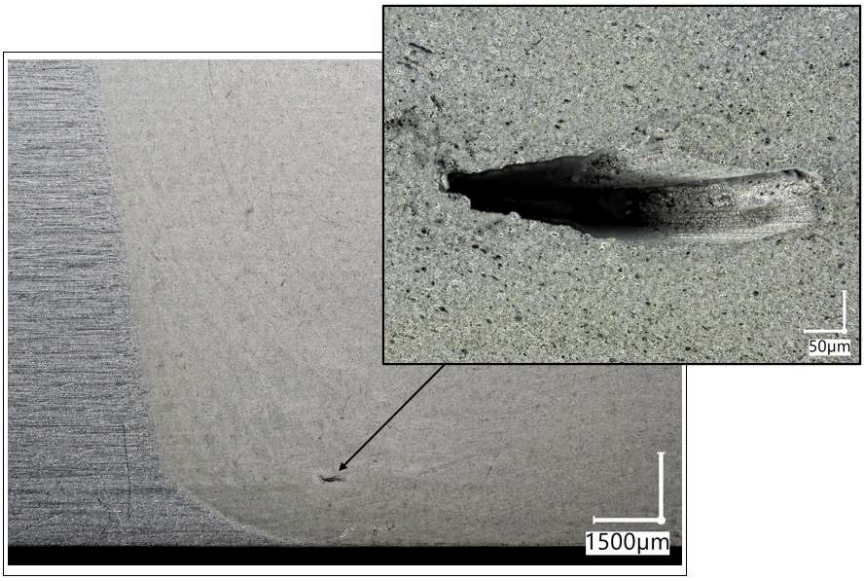

Figure 4. Image showing volumetric defect observed in a weld with low energy density (reference Figure 2).

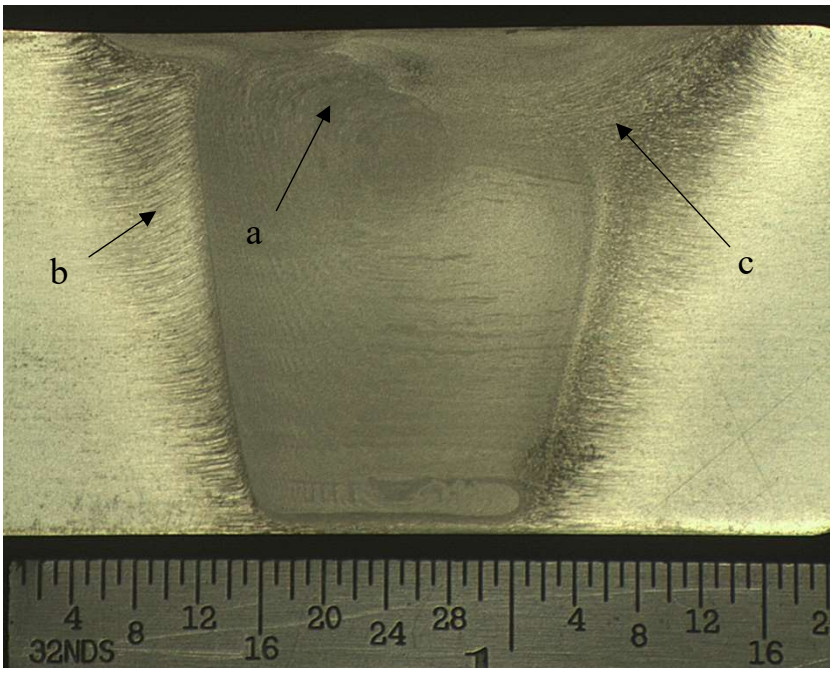

Figure 5. Macro section from weld made at 1.27 mm/s travel speed and 207 rev/min spindle speed (0.219 m/s average surface velocity), showing (a) non-uniform region in upper SZ (cross reference Figure 2), (b) upturned grains just outside the SZ and (c) influx of material from retreating side.

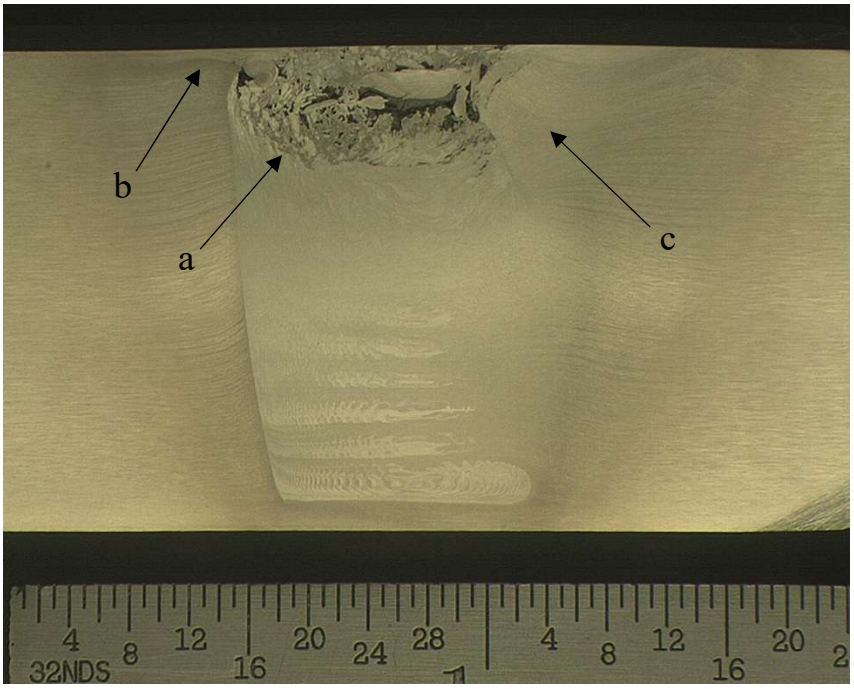

Figure 6. Macro section from weld made at 1.27 mm/s travel speed and 246 rev/min spindle speed (0.261 m/s average surface velocity), showing (a) volumetric defect in upper SZ (reference Figure 2), (b) minimal evidence of shoulder in SZ and (c) influx of material from retreating side.

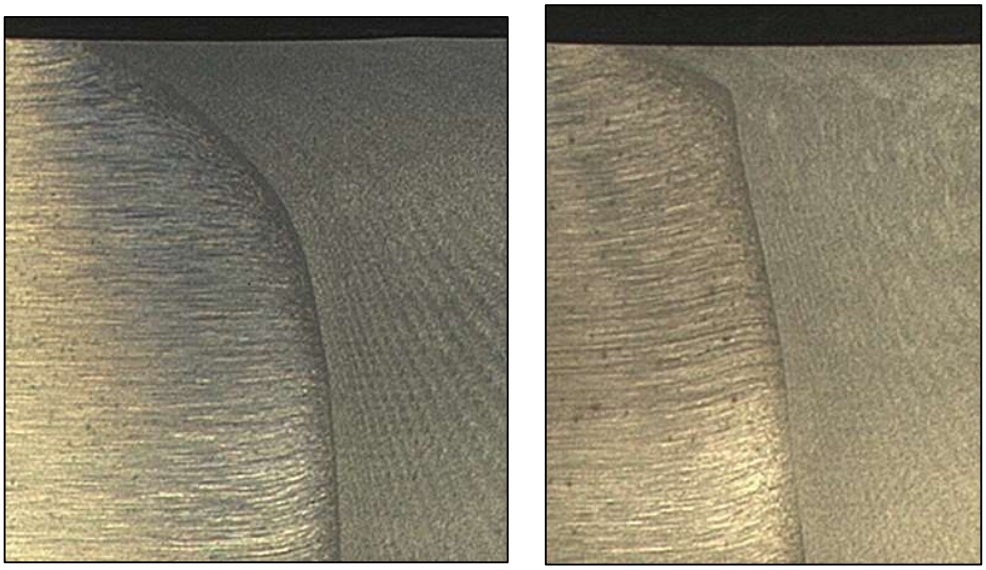

Figure 7. Change in upper advancing side SZ shape, general appearance at 0.157 m/s surface velocity and below (left), appearance at 0.178 m/s surface velocity and above (right).

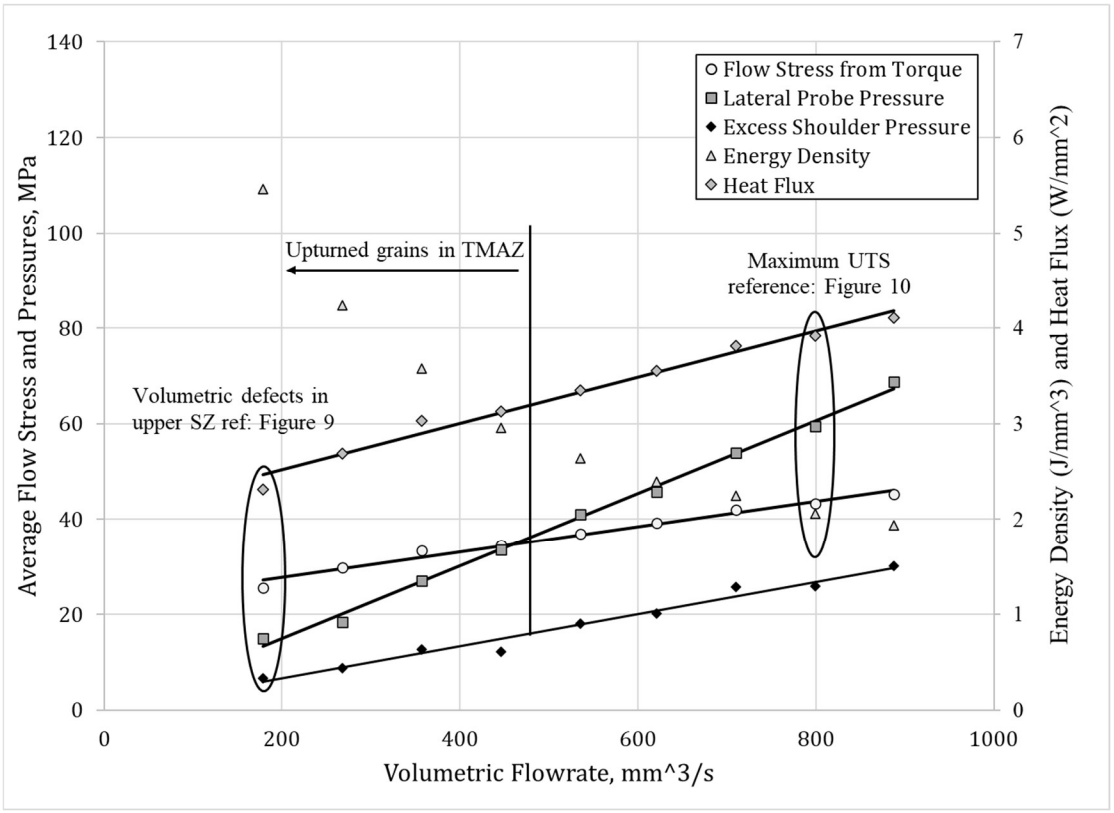

Figure 8. Test Series 2 average flow stress, lateral probe pressure, excess shoulder pressure, heat flux and energy density as a function of volumetric flowrate, from welds in 25-mm 7075-T6 aluminum, all made at 148 rev/min spindle speed (0.157 m/s average surface velocity), with all welds made in position control.

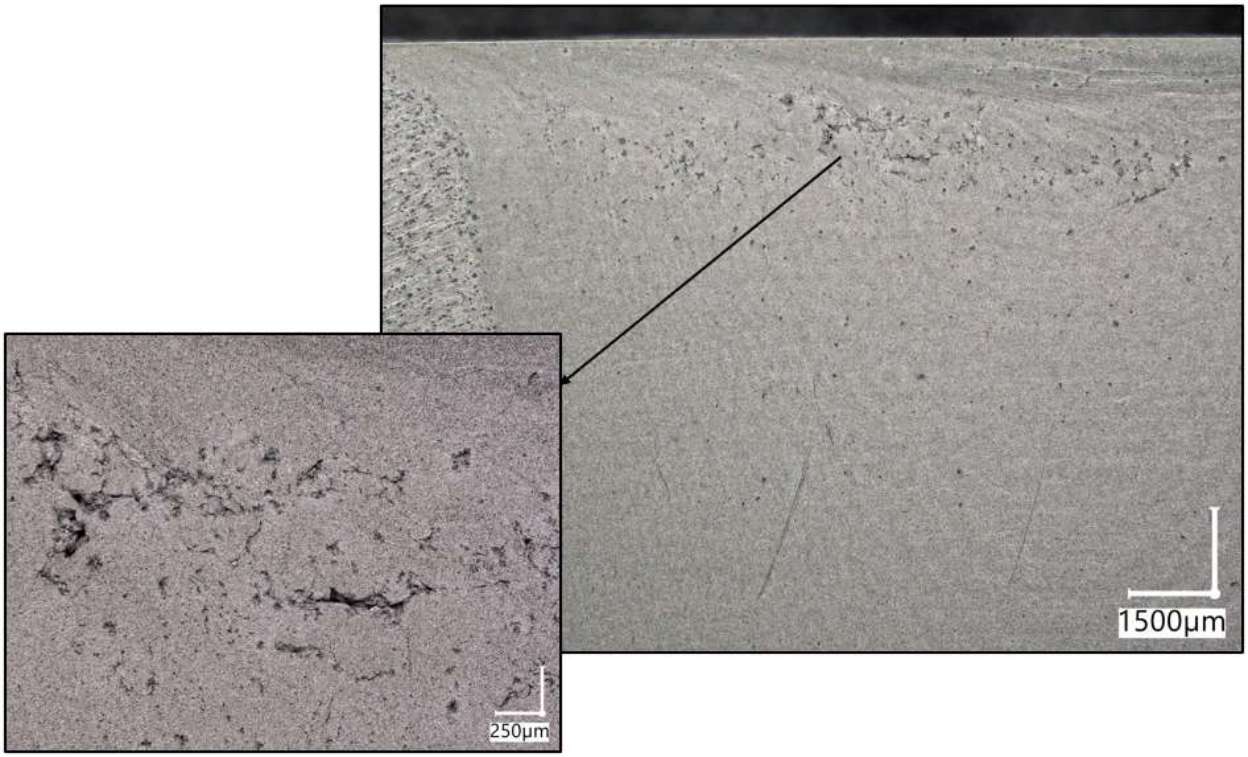

Figure 9. Macro section from a weld made at 148 rev/min spindle speed and 0.42 mm/s travel speed (178 mm^3/s volumetric flowrate), showing scattered volumetric defects in upper SZ (reference Figure 8).

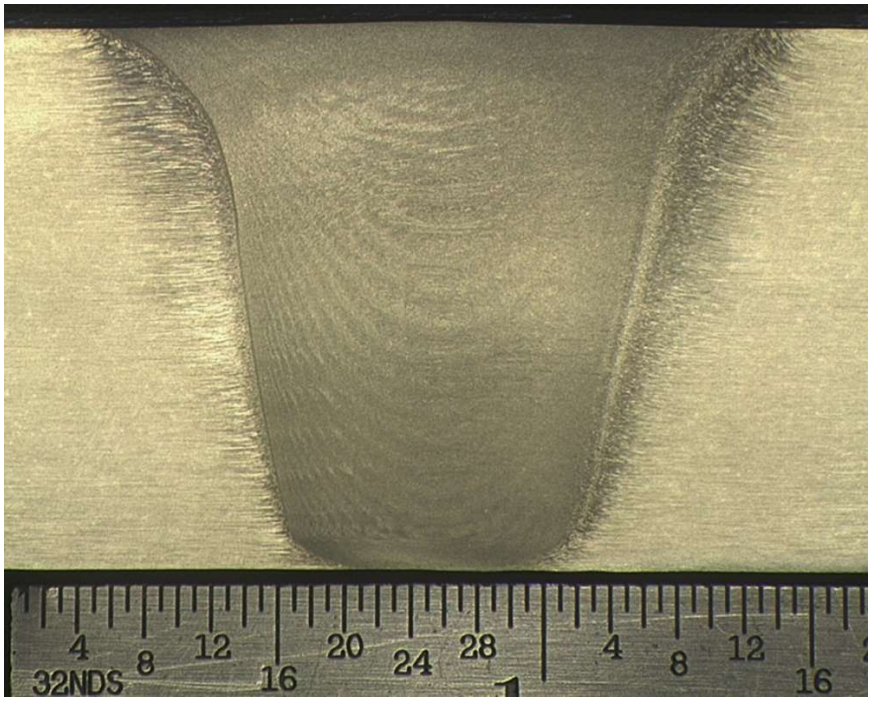

Figure 10. Macro section from a weld made at 1.91 mm/s travel speed (779 mm^3/s volumetric flow rate) and 148 rev/min spindle speed (0.157 m/s average surface velocity) which exhibited the maximum ultimate tensile strength of 440 MPa. Reference Figure 8.

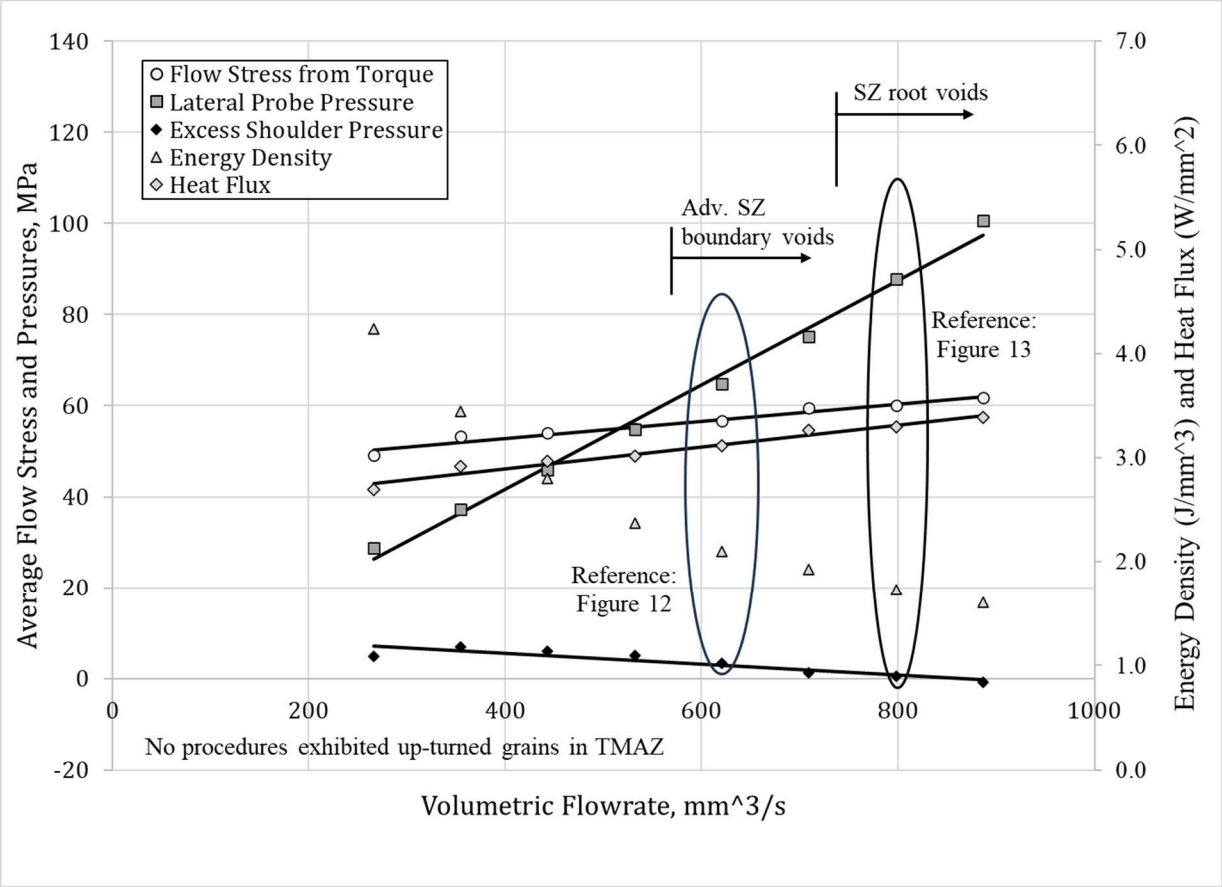

Figure 11. Test Series 3 average flow stress, lateral probe pressure, excess shoulder pressure and energy density from welds in 25-mm 7075-T6 aluminum, all made at 89 rev/min spindle speed (0.095 m/s average surface velocity), with welds made in load control only.

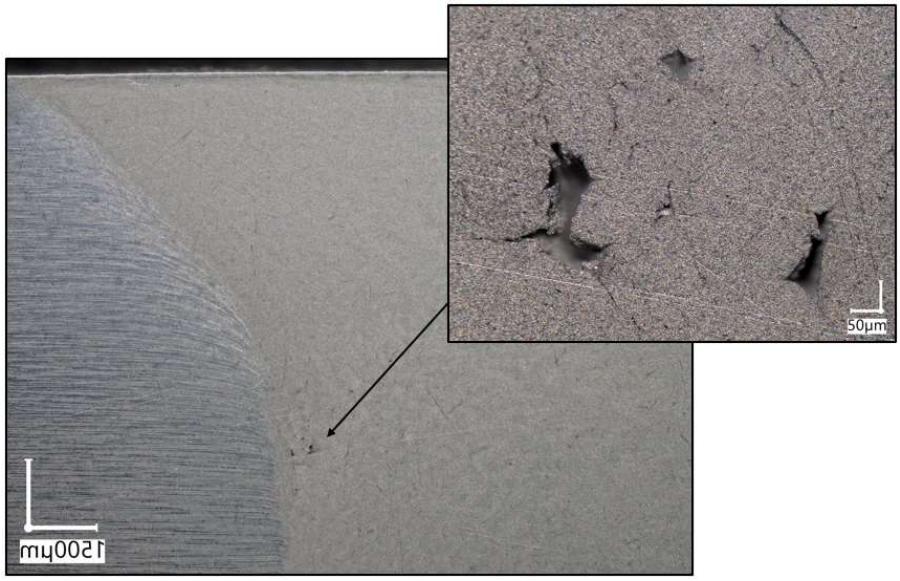

Figure 12. Macro section from a weld made at 1.48 mm/s travel speed (621 mm^3/s volumetric flowrate) and 89 rev/min spindle speed (0.095 m/s average surface velocity) with detail of advancing side SZ cluster of small volumetric defects.

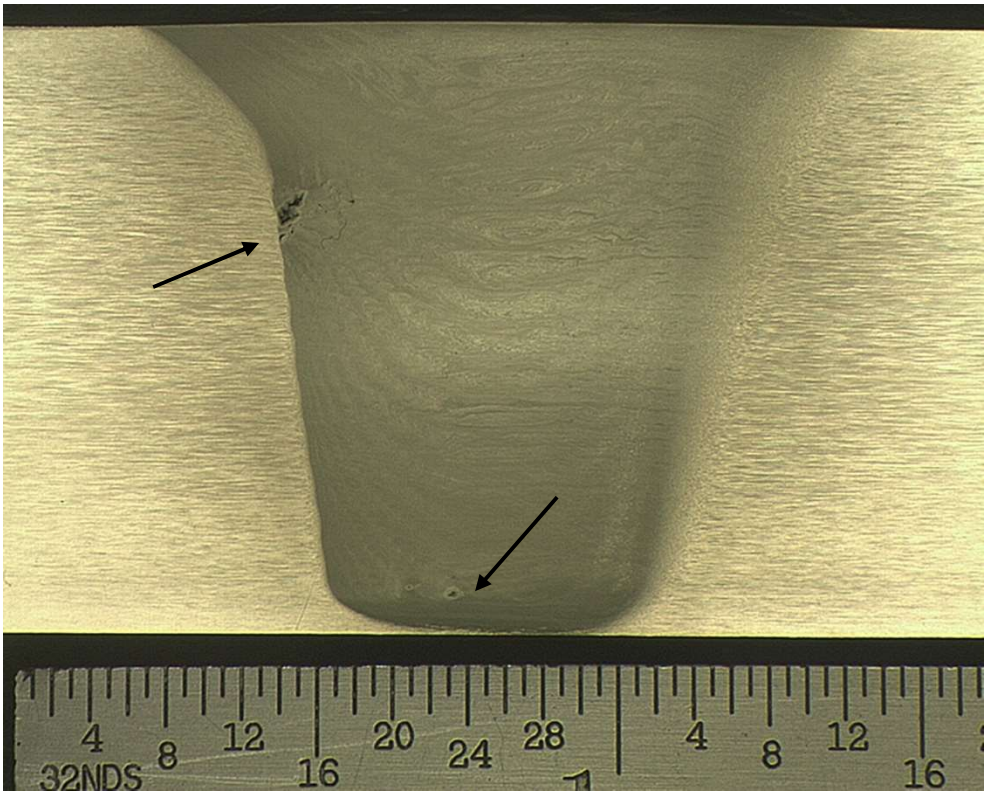

Figure 13. Macro section from a weld made at 1.91 mm/s travel speed (800 mm^3/s volumetric flow rate) and 89 rev/min spindle speed (0.095 m/s average surface velocity) which exhibited volumetric defects in the upper advancing side of the SZ and in the root of the SZ, as indicated.

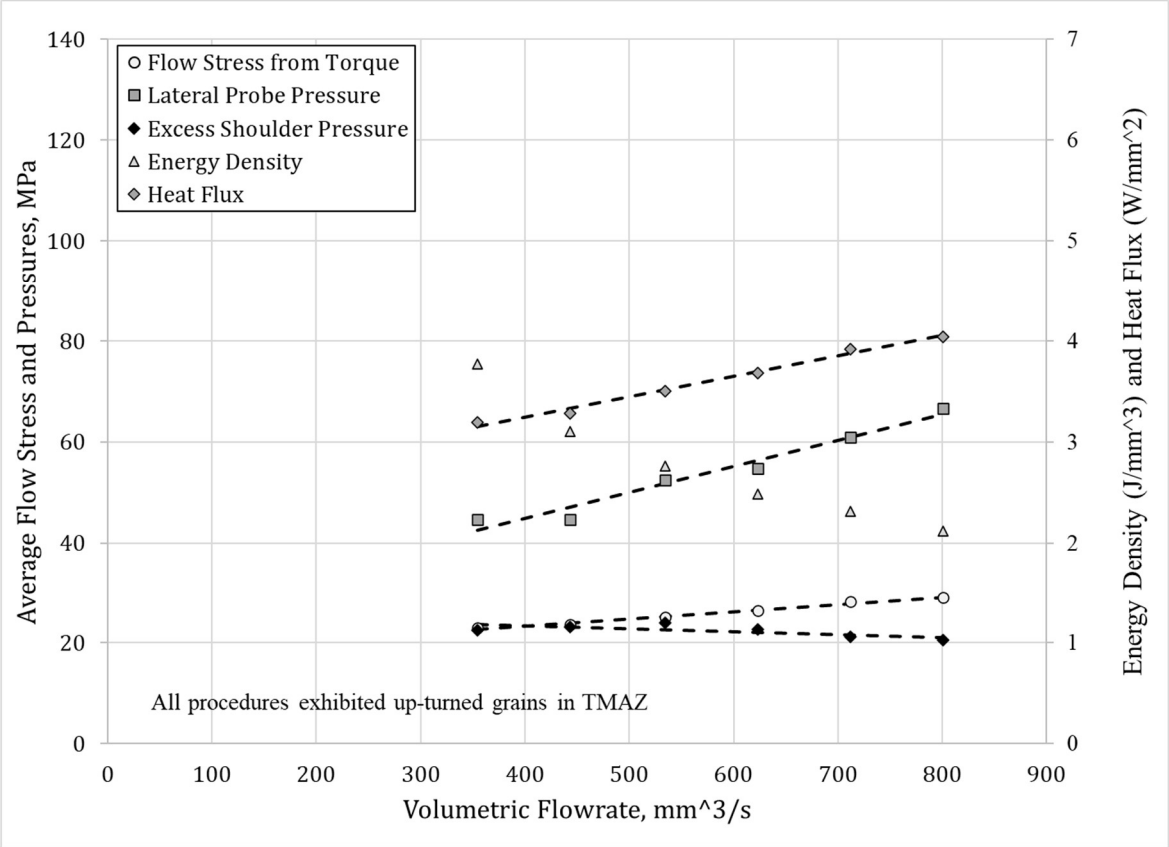

Figure 14. Test Series 4 average flow stress, lateral probe pressure, excess shoulder pressure, heat flux and energy density from welds in 25-mm 7075-T6 aluminum, all made at 227 rev/min spindle speed (0.240 m/s average surface velocity), made in load control. All welds had gross volumetric defects in the upper SZ, with severity decreasing with increasing welding speed.

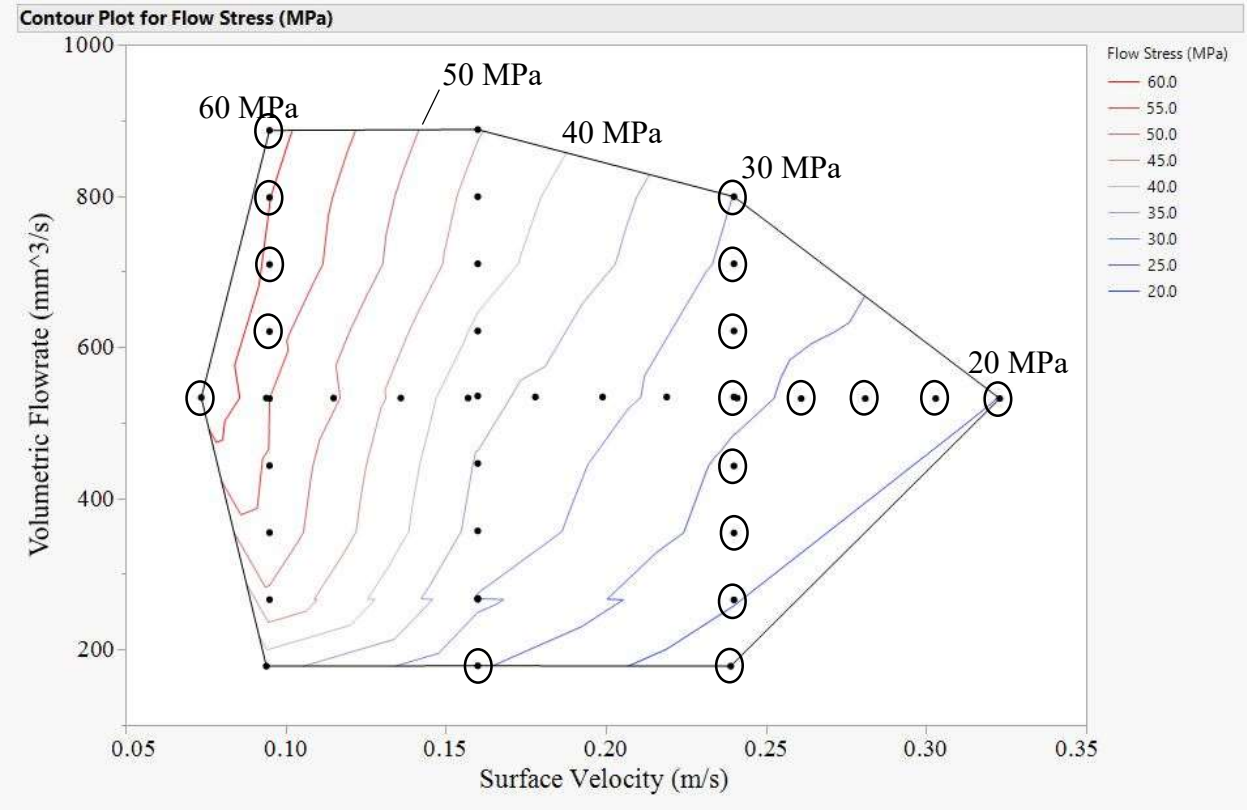

Figure 15. Contour plot of flow stress as a function of surface velocity and volumetric flowrate, procedures with volumetric defects indicated, 25-mm 7075-T6 FSW.